International Conference on Space Optics—ICSO 2018

Chania, Greece

9–12 October 2018

Edited by Zoran Sodnik, Nikos Karafolas, and Bruno Cugny

2.0 micron wavelength injection seed semiconductor laser for lidar transmitter for global-scale measurements of CO2

Siamak Forouhar

Ryan Briggs

Mahmood Bagheri

Clifford Frez

et al.

esa icso proceedings cnes

International Conference on Space Optics — ICSO 2018, edited by Zoran Sodnik, Nikos Karafolas, Bruno Cugny, Proc. of SPIE Vol. 11180, 111800U · © 2018 ESA and CNES · CCC code: 0277-786X/18/$18 · doi: 10.1117/12.2535949

2.0 μm wavelength injection seed semiconductor laser for lidar transmitter for global-scale measurements of CO2

*Siamak Forouhar, Ryan Briggs, Mahmood Bagheri, Clifford Frez; Mathieu Fradet
Jet Propulsion Laboratory, California Institute of Technology

* Corresponding author: siamak.forouhar@jpl.nasa.gov

ABSTRACT

Many of the high accuracy Earth science survey missions are planned to use laser-based remote sensing instruments. The 2-μm laser wavelength is of particular interest due to the presence of many CO_2 and H_20 absorption lines in its vicinity[1]. Transmitter architectures are typically composed of an optically pumped, frequency-stable, solid-state seed laser and a high-power optical amplifier.[2, 3] Taking advantage of the reliability and relative simplicity of semiconductor lasers, this architecture can substantially improve by replacing the solid-state light source with semiconductor lasers of comparable performance. This approach will greatly improve the system reliability, and will simplify instrument integration and space qualification. There are currently very limited semiconductor lasers operating in the 2-μm range with performance satisfactory enough for use as an injection seed in a laser absorption spectrometer. Optimally, seed lasers producing greater than 50 mW of continuous-wave (CW), with frequency jitter of less than 1 MHz are desired to reliably resolve the CO_2 absorption lines near 2-μm. In this paper, we report the demonstration of high-power, single-longitudinal-mode laterally coupled distributed feedback (LC-DFB) lasers at 2.05 μm wavelength. We measured more than 80 mW of CW power at -10 ºC for devices with a 4-μm-wide ridge and 2-mm-long cavity.

INTRODUCTION

Semiconductor lasers emitting near 2-μm wavelength have been demonstrated in both Indium Phosphide (InP) and Gallium Antimonide (GaSb) material systems. Due to Auger recombination and other loss mechanisms at longer wavelengths, state-of-the-art single-mode InP-based diode lasers operating at 2μm are limited to output powers near 10 mW. [4] GaSb-based laser materials are a promising alternative for greater than 2-μm lasers; [5] however, conventional fabrication of DFB lasers incorporating buried gratings for longitudinal mode selection is challenging due to the difficulty of epitaxial regrowth over GaSb alloys. An alternative method for DFB fabrication makes use of Bragg gratings etched alongside a ridge waveguide to form a laterally coupled distributed-feedback (LC-DFB) laser. [6] This approach enables fabrication of single-longitudinal-mode lasers using a single epitaxial growth process. To date, the power output of LC-DFB lasers using GaSb-based alloys has been limited to only a few milliwatts. In particular, previously demonstrated devices have relied on deposited metal gratings that provide strong feedback but generate additional absorption loss in the laser cavity. [7]

In this work, we report on high-power 2-μm laterally coupled etched grating distributed feedback (LC-DFB) lasers. The fabricated lasers produce more than 80 mW of single-mode output from the front facet with side-mode suppression greater than 20 dB. The devices also exhibit stable wavelength tuning over a broad range of temperature and operating current.

LASER DESIGN AND FABRICATION

The heterostructure laser wafer was grown using solid-source molecular-beam epitaxy on a *n*-GaSb substrate, with 1.5-μm-thick $Al_{0.85}Ga_{0.15}As_{0.07}Sb_{0.93}$ cladding layers. The nominally undoped $Al_{0.3}Ga_{0.7}As_{0.02}Sb_{0.98}$ waveguide layers were grown to a total thickness of approximately 800 nm with two 12.5-nm $In_{0.23}Ga_{0.77}As_{0.1}Sb_{0.9}$ quantum wells (QWs) centered in the waveguide and spaced 40 nm apart. The resulting compressive strain in the QWs is approximately 1.45%.[8] Ridges structures as shown in Fig.1 (a) were fabricated using contact lithography and inductively coupled plasma

reactive-ion etching. Second-order gratings with a pitch of 582 nm were patterned alongside the ridges using electron-beam lithography and etched to a depth of approximately 350 nm, shown in Fig. 1(b). We elected to implement second-order gratings because of the simplicity of fabricating larger grating features as well as the ability to suppress multimode operation around the stop band that arises from index-modulated DFB structures. The gratings were covered with 1 μm of SiN_x using plasma-enhanced chemical-vapor deposition prior to depositing gold contacts and cleaving the wafer into 2-mm-long bars. The exposed facets were passivated with a 10-nm layer of electron-beam evaporated Y_2O_3. One facet was further passivated with a thin layer of SiO_2, resulting in facet reflectivity of 30%, and the other facet was covered with a two-layer anti-reflection (AR) coating of TiO_2 and Al_2O_3. Using a calibrated Fourier-transform infrared (FTIR) spectrometer, the AR coating was found to have reflectivity of 2% at 2.05 μm on a silicon reference sample. Finally, individual lasers were mounted epitaxy-side up on gold-coated C-mount copper blocks.

Two-dimensional numerical calculations were used to determine the electric field distribution and modal effective index, n_{eff}, for the fabricated ridge waveguides.[9] Due to the thickness of the ridge and the SiN_x covering the gratings, the metal contacts contribute negligibly to n_{eff} for guided modes. Assuming an effective-medium index for the grating region, we find $n_{\text{eff}} = 3.53$ for the fundamental transverse-electric mode and an electric-field overlap factor of $\Gamma_{\text{grating}} = 0.33\%$ for the grating region. Using the approximation employed in Ref. 12, the feedback effect of the lateral gratings can be quantified by estimating the grating coupling coefficient,

$$\text{Eq. (1)} \qquad \kappa = \frac{\left(n_{\text{clad}}^2 - n_{\text{cover}}^2\right)}{n_{\text{eff}}\lambda} \frac{\sin\left(m\pi w/\Lambda\right)}{m} G_{\text{grating}}$$

where n_{clad} is the index of the $Al_{0.85}Ga_{0.15}As_{0.07}Sb_{0.93}$ cladding layer into which the gratings are etched, n_{cover} is the index of the SiN_x, Λ is the grating pitch, w is the width of the grating teeth, and $m = 2$ is the relevant grating diffraction order. For the fabricated devices, we measured $w = 265$ nm, corresponding to a duty cycle of $w/\Lambda = 0.46$ and an estimated κ of 3 to 4 cm^{-1}, which, for a cavity length of $L = 2$ mm, yields $\kappa L \sim 1$.

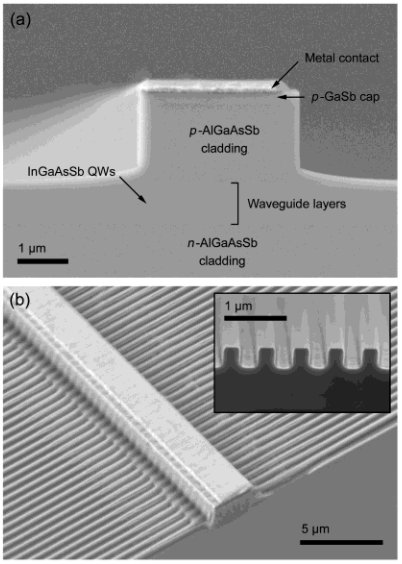

FIG. 1. (a) Cross-section scanning-electron micrograph of a 3-μm-wide laser ridge topped with a titanium-platinum-gold contact layer. (b) Top view of the LC-DFB laser structure, with a cross section of the grating shown in the inset. The micrographs show the device structure prior to deposition of the SiN_x cover layer on the gratings and electroplating of top gold contacts

LASER PERFORMANCE

The CW light-current-voltage characteristics and emission spectra for a LC-DFB laser with a 4-μm-wide ridge plotted in Fig. 2, where the laser emission collected from the AR-coated facet of the device. The solid portions of the power curves in Fig. 2(a) indicate the range of operating current for which single-mode DFB emission observed, while the dashed lines

correspond to multimode emission. At 10 °C, the laser exhibited a threshold current of 34 mA, and the total power conversion efficiency for emission from the AR-coated facet reached 11%. The inset in Fig. 2(a) shows a CW life test for a LC-DFB laser operated at a current of 300 mA.

The lasers operated in open air with a thermoelectric cooler for temperature stabilization at 20 °C. The device showed less than 3% variation in output power over a period of 1000 h, within the error of the thermopile detector. Figure 2(b) shows modal gain spectra obtained from sub-threshold Hakki-Paoli measurements, which include the effect of grating reflections near 2.053 μm. The spectra indicate total optical loss of approximately 18 cm^{-1}. With an estimated facet loss of 13 cm^{-1}, the internal waveguide loss is therefore approximately 5 cm^{-1}. The total loss is comparable to Fabry-Perot lasers without gratings fabricated with the same ridge geometry and facet coatings, indicating that, in contrast to LC-DFB devices with metal gratings, the etched gratings do not introduce significant broadband attenuation. From the characterization of the Fabry-Perot devices, we estimate internal quantum efficiency of 58%.

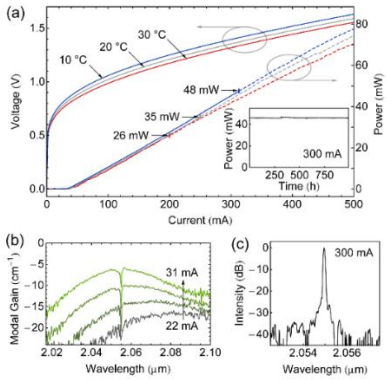

FIG. 2. (a) CW light-current-voltage characteristics for a 2-mm-long LC-DFB laser operated at various heat-sink temperatures. The solid portions of the power curves indicate the range of operating current for which single-mode DFB laser emission observed, while the dashed lines correspond to multimode emission. The inset shows output power collected over a period of several hundred hours from a LC-DFB laser operated at 300 mA. (b) Sub-threshold modal gain spectra for the LC-DFB structure measured at different currents in increments of 3 mA. (c) LC-DFB laser output spectrum showing single-mode operation at 300 mA.

The emission wavelength of the LC-DFB laser for a range of heat-sink temperature and operating current shown in Fig. 3. Only the peak wavelengths corresponding to DFB-mode output shown; therefore, the data points roughly define the upper bounds of current and heat sink temperature for single-mode operation. Previous studies have shown that the gain spectrum for GaSb-based laser materials shifts more rapidly than InP- or GaAs-based materials with increasing temperature. In particular, the emission wavelength for Fabry-Perot lasers made from the same active materials used here has been shown to tune at 1.39 nm/°C with a thermal resistance of 22.3 °C/W.[14]

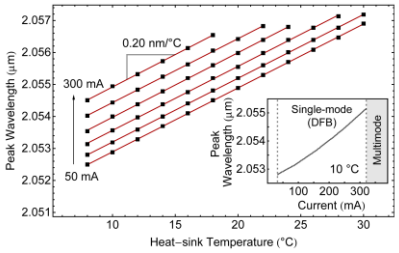

FIG. 3. Peak wavelength of LC-DFB laser emission as a function of heat-sink temperature collected at 50-mA current intervals. Within the current range shown, the peak laser emission wavelength tunes linearly with temperature at 0.20 nm/°C. Only data points corresponding to single-mode DFB operation are shown. The emission wavelength tunes continuously as the current is increased (inset), but the laser emission eventually becomes multimode due to shifting of the gain spectrum.

As indicated in Fig. 3, a broad temperature-current window exists within which the LC-DFB lasers exhibit stable and continuous wavelength tuning at 0.20 nm/°C, comparable to the tuning characteristics of GaSb-based LC-DFB lasers with metal gratings. Shown in the inset of Fig. 3, the peak wavelength for DFB operation, λ, as a function of current, I, is well fit by the expression $\lambda(I) = \lambda_0 + C_1 I + C_2 I^2$, with the parameters λ_0 = 2053.62 nm, $C_1 = 5.39\times10^{-3}$ nm/mA, and $C_2 = 7.94\times10^{-6}$ nm/mA^2; however, with increasing temperature and current, the relatively higher tuning rate of the gain spectrum leads to laser oscillation in Fabry-Perot modes away from the DFB wavelength.

The top portion of Fig. 4 shows LC-DFB emission spectra collected at 10°C with increasing current. The transition from single-mode DFB to Fabry-Perot operation can be seen between 300 and 350 mA, where the redshifted gain spectrum leads to laser oscillation at the DFB wavelength as well as at longer wavelengths. As shown in the inset, the longer-wavelength emission tunes by slightly more than 1 nm/°C, which is consistent with previous results obtained for Fabry-Perot lasers without Bragg gratings and indicates comparable thermal resistance. The lower portion of Fig. 4 shows the spectral emission and total power output for the same LC-DFB device measured in a cryostat at -10 °C. At low current levels, the gain spectrum is blueshifted from the DFB wavelength; however, current-induced heating results in a region of stable single-mode DFB operation above 500 mA, with output power from the AR-coated facet exceeding 80 mW CW (see lower inset, Fig. 4). At still higher current levels, we observed emission from longer-wavelength Fabry-Perot modes as the gain spectrum continued to shift toward longer wavelengths.

We measured LC-DFB laser linewidths of 1.4 MHz and 900 KHz for 500 ms and 10 ms observation times, respectively. The linewidths were derived from the frequency-noise power-spectral density measured using a Fabry-Perot interferometer.[10,11] The result is an upper bound of the linewidth that includes all components of instrumental noise, including mechanical jitter in the interferometer, amplitude noise of the voltage source tuning the interferometer, and noise in the laser current supply.

We have demonstrated high-performance, single-longitudinal-mode LC-DFB lasers at 2.05 µm wavelength. We measured more than 80 mW of CW power at -10 ºC for devices with a 4-µm-wide ridge and 2-mm-long cavity. This record performance is attributed to the high quality of epitaxial growth, device fabrication, and thermal management of the laser. These results are an important step toward the realization of high-power, frequency-stable semiconductor seed lasers suitable for lidar applications.

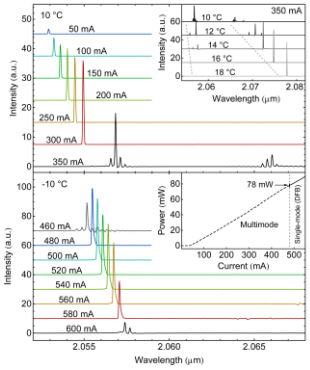

FIG. 4. (Upper panel) LC-DFB laser emission spectra for different current levels at a heat-sink temperature of 10 °C. Above 300 mA, laser oscillation in Fabry-Perot modes due to shifting of the gain spectrum to longer wavelengths. The inset shows the faster tuning rate of Fabry-Perot emission with increasing temperature.
(Lower panel) Emission spectra collected from the same device at -10 °C. At lower currents, emission is observed in Fabry-Perot modes; however, current-induced heated shifts the gain spectrum toward the wavelength corresponding to peak grating reflectivity, resulting in single-mode DFB operation between 500 and 600 mA. The inset shows the power emitted from the AR-coated facet at -10 °C, where the solid part of the curve corresponds to single-mode output.

ACKNOLEDGEMENT

This work was performed at the Jet Propulsion Laboratory (JPL), California Institute of Technology, under contract with the NASA. The authors thank G. Komar, J. Hyon and I. Eastwood for their support and encouragement.

REFERENCES

1. J. Caron and Y. Durand, Appl. Optics **48**, 5413 (2009).
2. G. D. Spiers, R. T. Menzies, M. Phillips, S. Geier, I. Poberezhskiy, and P. Meras, 14th Coherent Laser Radar Conference, Snowmass, CO (2007).
3. G. J. Koch, J. Y. Beyon, P. J. Petzar, M. Petros, J. Yu, B. C. Trieu, M. J. Kavaya, U. N. Singh, E. A. Modlin, B. W. Barnes, and B. B. Demoz, J. Appl. Remote Sens. **4**, 043512 (2010).
4. R. Phelan, J. O'Carroll, D. Byrne, C. Herbert, J. Somers, and B. Kelly, IEEE Photon. Technol. Lett. 24, 652–654 (2012).
5. L. Shterengas, G. L. Belenky, M. V. Kisin, and D. Donetsky, Appl. Phys. Lett. **90**, 011119 (2007).
6. S. Forouhar, R. M. Briggs, C. Frez, K. J. Franz, and A. Ksendzov, Appl. Phys. Lett. 100, 031107 (2012).
7. https://nanoplus.com/
8. J. A. Gupta, P. J. Barrios, J. Lapointe, G. C. Aers, C. Storey, and P. Waldron, IEEE Photon. Tech. Lett. **21**, 1532 (2009).
9. R. F. Kazarinov and C. H. Henry, IEEE J. Quant. Elect. QE-21, 144 (1985).
10. M. Bagheri, C. Frez, B. Kelly, J. A. Gupta, and S. Forouhar, Electron. Lett. 49, 1552 (2013).
11. M. Bagheri, G. D. Spiers, C. Frez, S. Forouhar, and F. Aflatouni, IEEE Photon. Technol. Lett. 27, 1934 (2015).